Castillo *et al. Int J Concr Struct Mater* (2022) 16:53
https://doi.org/10.1186/s40069-022-00540-w

International Journal of Concrete Structures and Materials

RESEARCH Open Access

Study on Early-Age Elastic Modulus of FRC Using Electrical Resistivity and Resonance Frequency

Daniel Castillo, Saman Hedjazi* and Ehsanul Kabir

Abstract

The correlation between surface electrical resistivity and modulus of elasticity of fiber-reinforced concrete (FRC) was studied within early ages in this study as a novel nondestructive method for predicting the modulus of elasticity of FRC. In addition to the relationship of the two quantities, the influence of various discrete fibers such as glass, nylon, polypropylene, and steel on the early age properties of FRC was investigated. Twenty-one FRC mixes were designed and tested; including four fiber types, three different fiber volume fractions for each fiber type, and three different water-to-cement ratios for all the different mixes. The surface electrical resistivity meter and resonance testing gauge were used to measure each specimen's surface electrical resistivity and modulus of elasticity. Early-age dynamic modulus of FRC may be predicted using the mechanical properties and dimension of the fiber, according to proposed mathematical calculations. Statistical analysis was performed on the experimental results and the results acquired by the proposed equations, to examine and proof the accuracy of the proposed equations. The acceptable coefficient of variation of 5–9 percent confirmed the good agreement between the measured and predicted values.

Keywords: NDT, modulus of elasticity, resonance frequencies, early age properties, electrical resistivity

1 Introduction

The elastic modulus of concrete is a critical quantity in the design of concrete structures because it affects both early-age and long-term deformations of structural members. When members are designed to be loaded at different ages, the modulus of elasticity must be calculated precisely to ensure the structural integrity (Suksawang et al., 2018). Structural members that must be built using rapid construction methods are loaded early in the construction process. As a result, a successful design is contingent on the accuracy of the assumed properties of materials at early ages. For example, in the cantilever construction method for prestressed bridge decks, where each new segment is installed on the previous recently installed segment and members are loaded at an early stage, an in-depth understanding of material characteristics is required at the initial stage to protect the structure from deformations. The early age is typically defined as the first 3–8 h or a few days following the casting of concrete (Kayondo et al., 2019). The amount of hydration achieved during this period determines the elastic modulus and mechanical properties of concrete which can be influenced by a variety of factors, including cement microstructure, specimen shape, mixture proportions, *w*/*c* ratio, fiber and additive inclusion, coarse aggregate vs. fine aggregate ratio, concrete age, and curing conditions (Chavhan & Vyawahare, 2015; Safiuddin et al., 2018). The elastic modulus of concrete can be determined empirically or calculated using a formula from various codes such as ACI 318 for plain concrete (Lee et al., 2015; Suksawang et al., 2018).

Journal information:ISSN 1976-0485 / eISSN 2234-1315

*Correspondence: shedjazi@georgiasouthern.edu

Department of Civil Engineering and Construction, Georgia Southern University, Statesboro, GA, USA

Fiber-reinforced concrete (FRC) is a widely used construction material that has a reputation for limiting the development and propagation of cracks due to its increased ductility and stiffness. ASTM C1116 classifies fiber-reinforced concrete (FRC) into four types based on the type of fiber used: steel, glass, synthetic, and natural fiber-reinforced concrete (American Society for Testing Materials, 2015a). The physical, chemical, and mechanical characteristics of fiber determine the mechanical properties of each form of FRC. The major properties that influence the performance of FRC include fiber type, dimensions, volume fractions, fiber–matrix bonds, elastic modulus, tensile strength, and chemical properties of concrete mixture (Dopko, 2018). Several studies have been carried out to predict the elastic modulus of FRC with different fiber types (Aslani & Natoori, 2013; Aslani & Samali, 2014; Ayub et al., 2016). FRC's elastic modulus has been shown to vary depending on the *w*/*c* ratio, coarse-to-fine aggregate ratio, fiber type, diameter, length, and volume fraction (Skazlić & Bjegović, 2009; Wtaife et al., 2018). However, the published experimental results and associated equations were unable to address the issue of having a unique equation that can be applied to any fibers.

Concrete specimens subjected to compression can provide a more accurate estimate of FRC's elastic modulus. But it is impractical for structures that are either under construction or already exist (American Society for Testing Materials, 2014; Shkolnik, 2005; Zeng et al., 2020). Earlier it was demonstrated that nondestructive testing (NDT) methods are more advantageous for estimating the static and dynamic modulus of elasticity in concrete because they are less expensive, safer, faster, and simpler to use (Estolano et al., 2018; Pokorny et al., 2016). However, the current equations for predicting FRC's elastic modulus do not account for fiber volume percent or fiber type. For example, ACI 318 connects elastic modulus and compressive strength and provides formulas for approximating elastic modulus that can be used for plain concrete (American Concrete Institute, 2014). Concrete's electrical resistivity, compressive strength, and elastic modulus are all inextricably linked to its hydration and microstructure formation. Shao et al. (2015) established a nonlinear relationship between the modulus of elasticity and the resistivity of concrete and proposed using electrical resistivity (ER) techniques to predict the elastic modulus of concrete, particularly at early ages. The elastic modulus of early age cemented gangue backfill columns was successfully determined using ER measurements (Guo et al., 2020). Teng et al. (2018) showed that ER testing can significantly help with the analysis of the elastic modulus and mechanical properties of high-performance hybrid FRCs. Chavez et al. (2014) developed a model that has predict the static modulus of elasticity using electrical resistivity values. An alternative method for determining the elastic modulus of concrete is the resonance test gauge (RTG), a vibration-based NDT test. Impact resonance was used to determine material properties such as dynamic elastic modulus to evaluate asphalt pavements for moisture damage (Yadav et al., 2021). For the determination of selected parameters such as thickness and dynamic modulus of elasticity of concrete structures, the resonant method was found reliable by Pokorny et al. (2016). Another study reported the elastic modulus of degraded concrete using resonant frequency to evaluate the distribution of damage at different depths within the concrete structure (Park et al., 2014). Using material constants such as elastic modulus and resonant frequencies, Kolluru et al. (2000) proposed mathematical models for concrete cylinders that are in good agreement with ASTM standard test procedures.

In this paper, the efficacy of nondestructive testing for detecting elastic modulus of concrete is studied. Twenty-one mixes in total were prepared comprising polypropylene, nylon, glass, and steel fibers at of 0.5 percent, 0.75 percent, and 1.00 percent fiber volume fractions (V_f); and *w*/*c* ratios of 40%, 45%, and 50%. This study was initiated to introduce a cost-effective and practical method that is reliable when used with FRC at young ages. The elastic modulus and electrical resistivity of FRC at an early age will also be investigated in relation to the *w*/*c* ratio, fiber volume percentage, and fiber type.

2 Experimental Program

A comprehensive experimental investigation was conducted to determine the dynamic modulus and electrical resistivity of FRC using four distinct fiber types, three volume fractions, and three *w*/*c* ratios as specified in Table 1. Nondestructive testing of FRC at early ages was performed using standard cylindrical molds ($4'' \times 8''$). The physical properties of the polypropylene, nylon, glass, and steel fibers used in this study are listed in Table 2. There are specific addition rates for each fiber type shown in Table 3 according to the manufacturer's specifications.

Twenty-one mixtures containing polypropylene, nylon, glass, and steel fibers at of 0.5 percent, 0.75 percent, and 1.00 percent fiber volume fractions (V_f); and *w*/*c* of 40%, 45%, and 50% were considered. For each mix ratio, 9 test cylinders were cast and cured, yielding 189 specimens. Table 4 shows the detailed mixture parameters, where CA represents coarse aggregate, FA represents fine aggregate, and W represents the total weight of FRC in cumec. Electrical resistivity and resonance frequency tests were performed after 1, 3, 7, and 28 days of curing.

Table 1 Materials, methods, and mix parameters for experimental investigation.

Testing	Mechanical property evaluated	Modulus of elasticity
	Nondestructive methods	Electrical resistivity and resonance frequency
Materials	Portland cement	Cement type I/II
	Maximum coarse aggregate size	0.1875 inch (4.7625 mm)
	Fiber types investigated	Polypropylene, nylon, glass, and steel
	Cylindrical molds	4-inch × 8-inch (100 × 200 mm)
Mixture parameters	V_f (%)	0.5, 0.75, and 1.0
	w/c ratio	0.40, 0.45, and 0.50
	Curing (days)	1,3,7, and 28

Table 2 Physical properties of four different types of fiber.

	Polypropylene	Nylon	Glass	Steel
Density, ρ (kg/m^3)	910	1150	2700	7800
Tensile strength, τ (MPa)	410	300	2000	1030
Flexural strength, σ (GPa)	5.6	2.8	77	203
Fiber length, l (mm)	19	19	13	25.4
Diameter of fiber, d (mm)	1.52	0.038	0.014	1.18

2.1 Specimen Preparation

ASTM C511 and ASTM C192 standards were followed when storing and curing concrete cylinders in the laboratory prior to testing (American Society for Testing Materials, 2002). At the Georgia Southern Concrete Research Lab, specimens were stored in a concrete curing tank of 103-gallon capacity made of galvanized steel. The curing tank is connected to a heater which keeps the water temperature in the curing tank stable for proper curing of concrete specimens. To prevent moisture loss, concrete cylinders were initially stored for up to 48 h at temperatures ranging from 60 to 80° F. Then cylinders were submerged in the curing tank after removing the plastic molds and kept at a temperature of 73.5 ± 3.5° F until the test date. According to ASTM C128 and C127, the specific gravity of both coarse and fine aggregates was calculated in order to alter the quantity of bath water used (American Society for Testing Materials, 2015b; 2015c).

2.2 Nondestructive Testing

2.2.1 Electrical Resistivity Measurement

The surface electrical resistivity of concrete cylinders was measured using the four-point Wenner probe method. A commercially available equipment named Resipod manufactured by Proceq SA, Switzerland (Gowers & Millard, 1999) was used. The concrete resistivity meter had a probe spacing of 38 mm (1.5″). The measurements were taken by placing four equidistant electrodes on the concrete surface in the longitudinal direction. This method involves passing an alternating current through the two outer probes and measuring the potential difference between the two inner probes. Because the ions are carried by the liquid through the concrete pores, the resistivity value is dependent on the probe spacing (Resipod User's Manual, 2017). The calibration of the equipment was checked before taking measurements for each mix specimen. For each concrete cylinder's circular face, readings were recorded at 0, 90, 180, and 270 degrees, and the results were averaged. Measurements were taken at 1, 3, 7, and 28 days for the 4-inch × 8-inch (100 × 200 mm) cylinders. Test specimens were removed from water tank after specific curing days and tested at saturated surface dry (SSD) condition at 23 ± 2 °C as specified in AASHTO T358 (American Association of State Highway & Transportation Officials, 2014). The surface electrical resistivity values were directly obtained in Kohm-cm from the Resipod output.

2.2.2 Resonance Frequency Measurement

The dynamic modulus of each specimen was determined using an ASTM C215-compliant (American Society for Testing Materials, 2019) resonant test gauge (Model: RTG-1) manufactured by Olson Instruments, Inc. United States. The dynamic modulus was determined by the impact resonance method using the longitudinal configuration after the specimens were cured in water for the specified 1-, 3-, 7-, and 28-days period. The dynamic

Table 3 Fiber addition rate according to fiber type and manufacturer specifications (Nycon, 2019).

Addition rate	Polypropylene	Nylon	Glass	Steel
Plastic shrinkage cracking	0.9 kg/m^3	0.6 kg/m^3	0.30–0.60 kg/m^3	10–15 kg/m^3
Performance of structure	N/A	N/A	5–15 kg/m^3	15–80 kg/m^3

Table 4 Concrete mix ratio for different fiber types.

Name	Fiber incorporated	V_f (%)	Fiber (kg/m^3)	C (kg/m^3)	CA (kg/m^3)	FA (kg/m^3)	W (kg/m^3)	*w/c*
Mix ID—1	None	0.00	0.0	503.3	709.7	986.5	201.3	0.40
Mix ID—2	Polypropylene	0.50	4.5	500.8	706.1	981.5	200.3	0.40
Mix ID—3		0.75	6.8	499.5	704.3	979.1	199.8	0.40
Mix ID—4		1.00	9.1	498.3	702.6	976.6	199.3	0.40
Mix ID—5		0.75	6.8	487.3	687.1	955.0	219.3	0.45
Mix ID—6		0.75	6.8	475.6	670.6	932.1	237.8	0.50
Mix ID—7	Nylon	0.50	5.7	500.8	706.1	981.5	200.3	0.40
Mix ID—8		0.75	8.5	499.5	704.3	979.1	199.8	0.40
Mix ID—9		1.00	11.4	498.3	702.6	976.6	199.3	0.40
Mix ID—10		0.75	8.5	487.3	687.1	955.0	219.3	0.45
Mix ID—11		0.75	8.5	475.6	670.6	932.1	237.8	0.50
Mix ID—12	Glass	0.50	13.5	500.8	706.1	981.5	200.3	0.40
Mix ID—13		0.75	20.2	499.5	704.3	979.1	199.8	0.40
Mix ID—14		1.00	27.0	498.3	702.6	976.6	199.3	0.40
Mix ID—15		0.75	20.2	487.3	687.1	955.0	219.3	0.45
Mix ID—16		0.75	20.2	475.6	670.6	932.1	237.8	0.50
Mix ID—17	Steel	0.50	39.0	500.8	706.1	981.5	200.3	0.40
Mix ID—18		0.75	58.5	499.5	704.3	979.1	199.8	0.40
Mix ID—19		1.00	78.0	498.3	702.6	976.6	199.3	0.40
Mix ID—20		0.75	58.5	487.3	687.1	955.0	219.3	0.45
Mix ID—21		0.75	58.5	475.6	670.6	932.1	237.8	0.50

modulus of test cylinders (4-inch × 8-inch) in GPa was calculated using an average of three longitudinal frequency measurements. An accelerometer and a hammer strike are positioned parallel to one another in the resonance test method. The accelerometer is connected to a specimen, which is then struck with a tiny hammer to determine the specimen's impact resonance. The specimen's resonant frequency is not discernible in the time domain, but it can be seen clearly in the frequency range. As a result, the resonant frequency peak was located by fast Fourier transform (FFT). The results are affected by specimen geometry, material properties, accelerometer attachment points, and hammer strike locations (Olson Instruments, 2020).

3 Revised Equations for FRC

In the literature, the modulus of elasticity for plain concrete is predicted (Shao et al., 2015):

$$E_c = a(\eta + b)^c + d, \tag{1}$$

where E_c is elastic modulus and η is electrical resistivity. The *w/c* ratio, cement, coarse and fine aggregate denote the parameters *a*, *b*, *c*, and *d* in Eq. (1). *C* is equal to 0.5 or 0.33.

When different types of fibers (steel, nylon, polypropylene, or glass) are added to concrete the electrical, physical, and mechanical properties of concrete change. Therefore, Eq. 1 is not applicable for FRC. To forecast the dynamic modulus of elasticity at early ages, Eq. 2 was devised. First, two points on the graph were identified by selecting the x and y-intercept from the curves for each fiber and curing days. To minimize round-off error, these two points were chosen as far apart as possible. Since none of the data points had the origin as a coordinate, both points are substituted into two equations of the form $f(x) = a(b)^x$. Finally, the resulting system was solved of two equations in two unknowns to find a and b to form an exponential function based on volume fractions of fiber ranging from 0.5 to 1% of volume and *w/c* ranging from 40 to 50% for all different mixtures including PFRC, NFRC, GFRC, and SFRC. At a young age, the growth in dynamic modulus and electrical resistivity is exponential (Haque & Rasel-Ul-Alam, 2018; Safari, 2016). As a result, an exponential equation is used to estimate FRC's dynamic modulus at an early age.

For G, P, and NFRC

$$E_d = \alpha e^{0.05*\eta t}. \tag{2}$$

For SFRC

$$E_d = \alpha e^{-0.037*\eta t}, \tag{3}$$

where η is the electrical resistivity ($k\Omega * \text{cm}$), t is the age (days), and α is determined using Eq. 3.

For polypropylene, nylon, and glass fibers

$$\alpha = 1.8\left(\frac{\sigma}{l/d}\right) + t^{0.95(\frac{\tau}{\rho})} + 19. \quad (4)$$

For steel fiber,

$$\alpha = 1.8\left(\frac{\sigma}{l/d}\right) + t^{7.5(\frac{\tau}{\rho})} + 19, \quad (5)$$

where flexural strength (σ) is expressed in GPa, fiber length (l) is in mm, diameter (d) will be also in mm, age (t) in days, tensile strength (τ) is expressed in MPa, and density (ρ) is expressed in kg/m^3.

In order to get the static modulus from the dynamic modulus, we may utilize Eq. 4 (Trifone, 2017):

$$E_c = 0.83E_d. \quad (6)$$

E_c is the static and E_d is the dynamic modulus of FRC in GPa, respectively.

To quantify the variability between the observed dynamic modulus (using the resonance test gauge (RTG method) and the projected dynamic modulus (using the electrical resistivity (ER) method) for each kind of fiber at the ages of 3 and 7 days, the COV (coefficient of variation) was introduced using Eqs. 5 and 6 (Wtaife et al., 2018):

$$COV = \frac{\sqrt{\frac{1}{n-1}\sum_{i=1}^{n}\left(f_{cpi}^{'} - f_{ci}^{'}\right)^2}}{\mu}, \quad (7)$$

$$\mu = \frac{\sum_{i=1}^{n} f_{ci}^{'}}{n}. \quad (8)$$

4 Results and Discussion

The findings of this study are reported in this section. By comparing experimental data to empirical data from Eq. 2, it was established that the new equation is more appropriate for FRC. All the fibers studied in this study showed excellent agreement between their experimental findings and those predicted by the equation. COV for each kind of fiber is also determined.

4.1 Influence of Fiber Volume Fraction and *w/c* Ratio on Electrical Resistivity of FRC

Fig. 1 depicts the ER vs w/c and V_f for all the FRC's tested in this study. Fig. 1A–D displays ER (kΩ * cm) versus V_f (0.5–1.0% vol.) for NFRC, PFRC, SFRC, and GFRC, respectively, at the ages of 1, 3, 7, and 28 days. Fig. 1E–H displays ER versus w/c ratio (0.4–0.5) for NFRC, PFRC, SFRC, and GFRC, respectively, at the ages of 1, 3, 7, and 28 days. Fig. 1A shows adding Nylon fibers to concrete gives rise to ER up to the threshold limit of this investigation (1.0% vol.) at all ages because nylon fibers are non-conductive and absorb water. Therefore, high fiber volume fractions of nylon fiber reduce the water-to-cement ratio resulting in higher ER.

Fig. 1B shows that the ER of PFRC reduces when fibers are added up to the threshold limit of this investigation at all ages despite being a non-conductive fiber because polypropylene fibers have the lowest specific gravity. Therefore, more strands of polypropylene fibers were added to the mix than any other fiber type. Having so many strands of polypropylene fibers reduced concrete workability, reduced concrete homogeneity, increased void content, and decreased electrical resistivity (Tapkın, 2008; Wang et al., 2021). Fig. 1C depicts that the ER of SFRC decreases with adding fibers up to the threshold limit of this investigation at all ages which is a result of steel fibers being conductive and rigid. Therefore, the rigid non-conductive fibers caused fiber balling which reduced the workability of concrete, increased void content, and decreased the electrical resistivity. Fig. 1D reveals that the ER of GFRC remains almost constant with the addition of fibers up to the threshold limit of this investigation because glass fibers are non-conductive but reduced the workability of concrete. Therefore, adding high fiber volume fractions of non-conductive glass fibers increased electrical resistivity but adding high amounts of fibers caused fiber balling which reduced the workability of concrete and electrical resistivity. Fig. 1D–H depicts that the ER of all types of FRC in this investigation decreases with the increases in w/c because as the water content increases the cement content decreases and having a lower cement content results in lower electrical resistivity. Finally, due to the hydration process, the electrical resistivity of all test samples increased with age, disregarding V_f and w/c ratio.

4.2 Influence of Fiber Volume Fraction and *w/c* Ratio on Elastic Modulus of FRC

Fig. 2 depicts Ed versus w/c and V_f ratio for all kinds of FRC investigated in this study. The dynamic modulus was influenced by the properties of the fiber incorporated. This could be due to the increased porosity of concrete because of fiber incorporation (Banyhussan et al., 2019). Steel fibers had the best flexural and tensile strength followed by glass, polypropylene, and nylon fibers, respectively. Therefore, SFRC had the highest dynamic modulus followed by GFRC, PFRC, and NFRC, respectively, as shown in Fig. 2A–D at all ages. The impact of the w/c

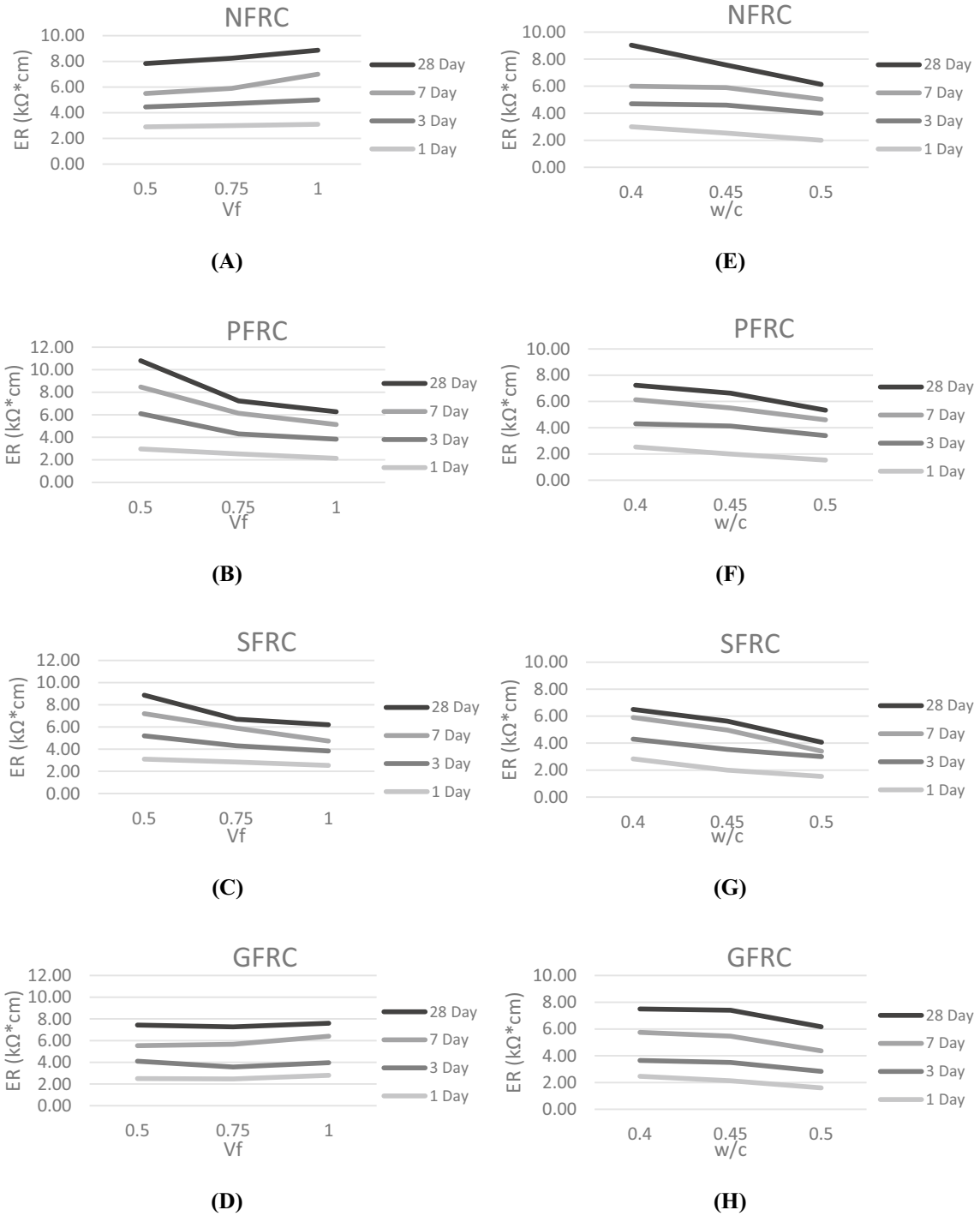

Fig. 1 **A–D** Effect of volume percentage (V_f) on electrical resistivity of FRC; **E–H** Effect of *w/c* ratio on electrical resistivity of FRC

on the dynamic modulus of FRC is demonstrated in Fig. 2E–H. It is observed that despite fiber type or age, the dynamic modulus of FRC decreases with the decrease in *w/c* ratio because there is less cement in the mix. Again, lower elastic modulus has no effect on flexural and tensile strength of fibers because it is only useful in bridging micro-cracks (Banyhussan et al., 2019).

For GFRC with a *w/c* ratio of 0.4, values for the elastic modulus fluctuated at the early age. However, the variation in all other fiber types remained consistent during

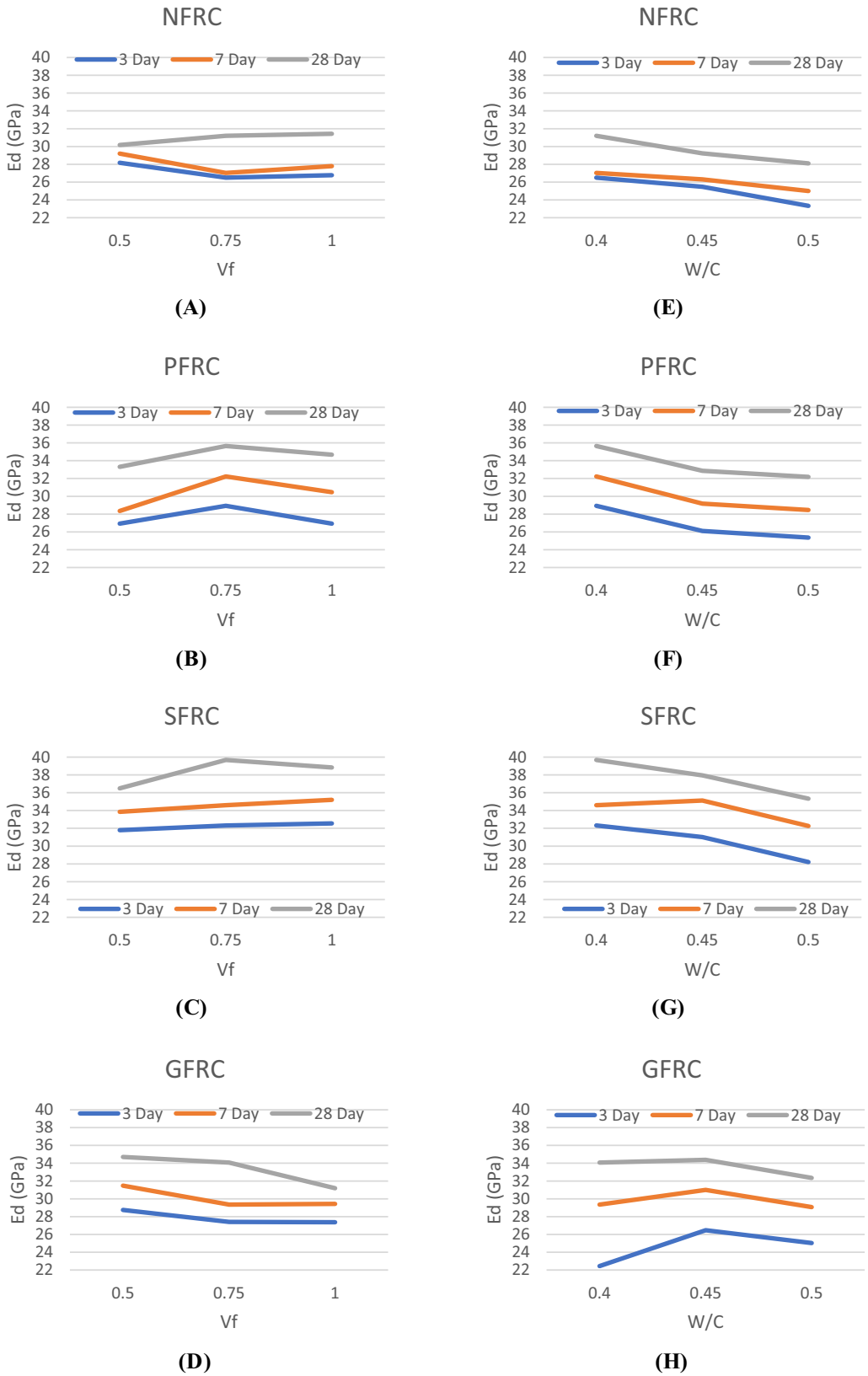

Fig. 2 **A–D** Effect of fiber volume percentage (V_f) on dynamic modulus of FRC; **E–H** Effect of *w/c* ratio on dynamic modulus of FRC

early age for concrete containing polypropylene, nylon, and steel, regardless of fiber volume fraction or water-to-cement ratio. The formation of micro-annuli around the FRC results in higher electrical modulus early in the curing process, which persists as curing progresses into the later stages due to the hydration reaction of cement paste (Appah & Reichetseder, 2001; Danjuschewskij & Ghofrani, 1991).

4.3 Relationship Between Electrical Resistivity and Elastic Modulus for PFRC

Fig. 3 depicts the relationship between PFRC's dynamic modulus (Ed) and electrical resistivity (ER) at 3 and 7 days. The predicted ER was computed using the proposed Eq. 2 and adjustment coefficients for PFRC.

All the data points from mixes containing polypropylene fibers (M7–M11) were used to establish a good correlation between PFRC's measured Ed and measured ER while considering V_f between 0.5 and 1.0% and w/c between 40 and 50%. The 3-day measured Ed and ER of PFRC range from 25 to 27 GPa and 3.3–6.2 kΩ * cm, respectively. The 7-day measured Ed and ER of PFRC range from 29 to 31 GPa and 4.5–8.6 kΩ * cm, respectively.

The COV was established to explain the discrepancy between Ed's observed and anticipated values. At 45 degrees, the measured and projected values are perfectly correlated, allowing the Keynesian Cross or the 45-degree line to be used to determine the equilibrium value (Blinder, 2008). The data points above and below this 45-degree line show conservative and non-conservative deviations, respectively (Yuan, 2015). Fig. 4 contains three scatter plots comparing PFRC's measured Ed (x-axis) to its predicted Ed (y-axis) in GPa at the ages of 3, 7, and 28 days. The calculated COV's were lower at 3 and 7 days of age.

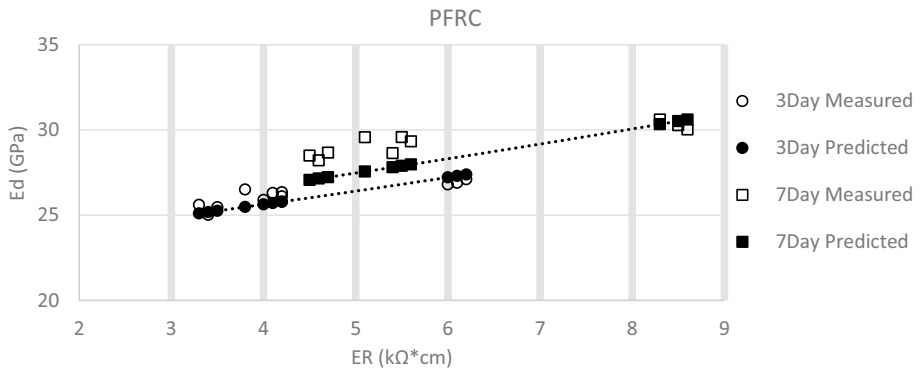

Fig. 3 Correlation between dynamic modulus and electrical resistivity for PFRC.

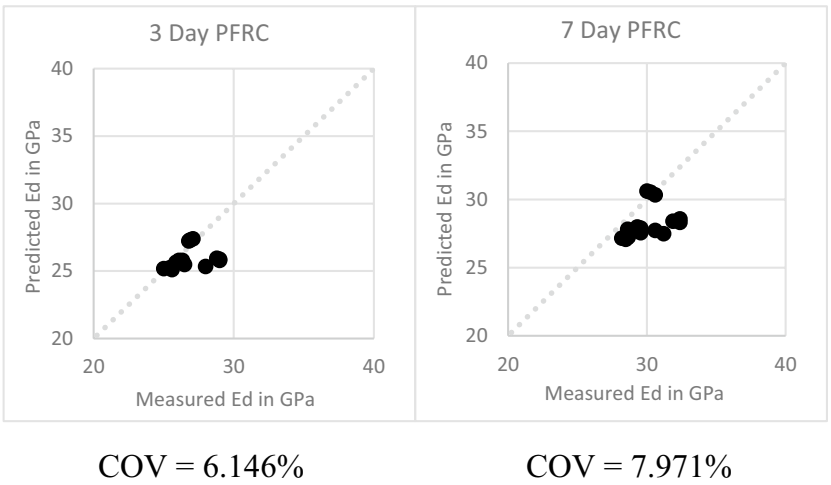

Fig. 4 Correlation between observed Ed and projected Ed for PFRC at early ages.

4.4 Relationship Between Electrical Resistivity and Elastic Modulus for NFRC

Fig. 5 depicts NFRC's dynamic modulus (Ed) versus electrical resistivity (ER). The measured data points belong to all mixes containing nylon fibers (M2–M6) and the predicted data points were obtained using the adjustment coefficients for NFRC.

The 3-day measured Ed and ER of NFRC range from 23 to 29 GPa and 3.9–5.3 kΩ * cm, respectively. The 7-day measured Ed and ER of NFRC range from 25 to 31 GPa and 5.0–7.0 kΩ * cm, respectively.

NFRC's measured Ed to its predicted Ed is presented in Fig. 6. The COV's at 3 and 7 days show that the proposed Eq. 2 works correctly at these ages.

4.5 Relationship Between Electrical Resistivity and Elastic Modulus for SFRC

Fig. 7 shows SFRC's dynamic modulus (Ed) versus electrical resistivity (ER). The measured data points are achieved from all mixes containing steel fibers (M12–M16) and the predicted data points were obtained using the adjustment coefficients for SFRC.

The 3-day measured Ed and ER of SFRC range from 31.5 to 33.1 GPa and 3.7–5.4 kΩ * cm, respectively. The 7-day measured Ed and ER of SFRC range from 33.5 to 37.0 GPa and 4.8–7.3 kΩ * cm, respectively.

SFRC's measured Ed to predicted Ed is depicted in Fig. 8. The axis, units, ages, and significance of the 45-degree dotted line are consistent with those in Fig. 3. The COV is low between the ages of 3 and 7 days which indicates that the proposed equation is valid for early age SFRC.

4.6 Relationship Between Electrical Resistivity and Elastic Modulus for GFRC

Fig. 9 presents GFRC's dynamic modulus (Ed) to its electrical resistivity (ER). However, the measured data points belong to all mixes containing glass fibers (M17–M21)

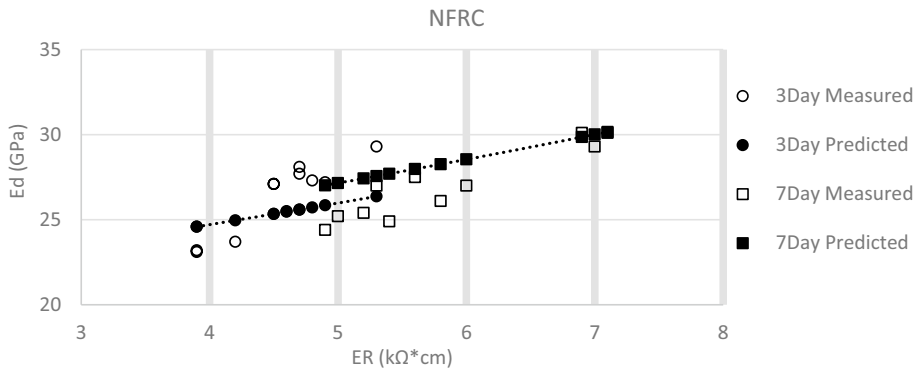

Fig. 5 Correlation between dynamic modulus and electrical resistivity for NFRC.

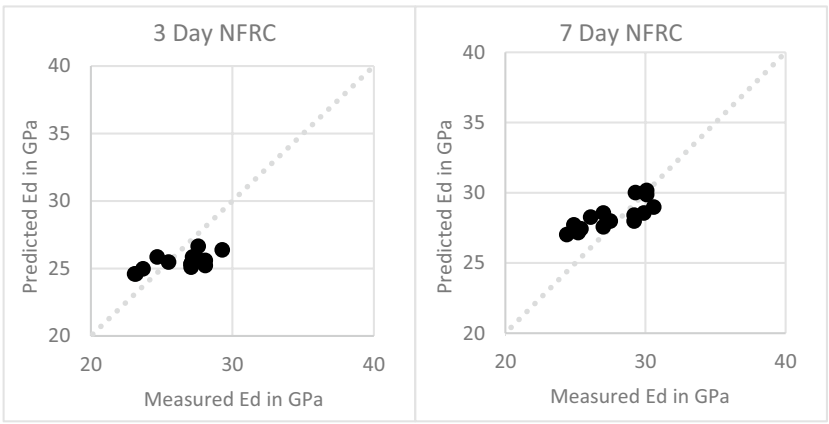

COV = 7.186% COV = 5.989%

Fig. 6 Correlation between observed Ed and projected Ed for NFRC at early ages.

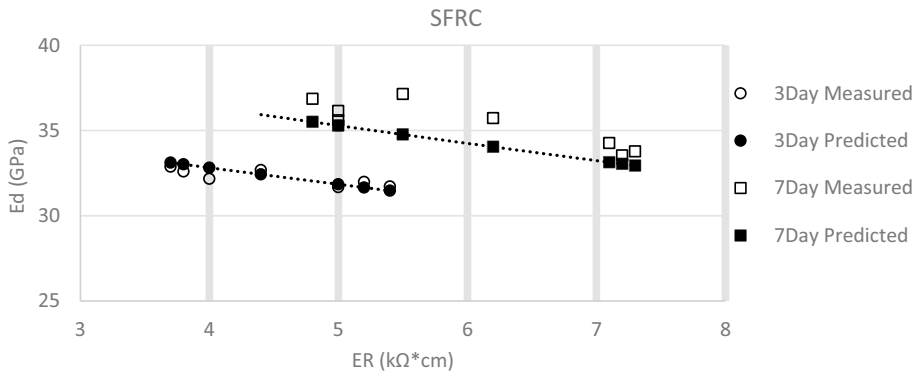

Fig. 7 Correlation between dynamic modulus and electrical resistivity for SFRC.

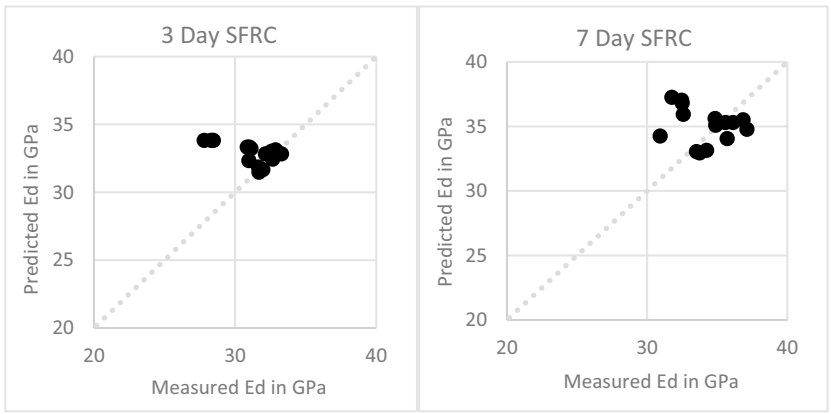

COV = 9.093% COV = 7.952%

Fig. 8 Correlation between observed Ed and projected Ed for SRFC at early ages.

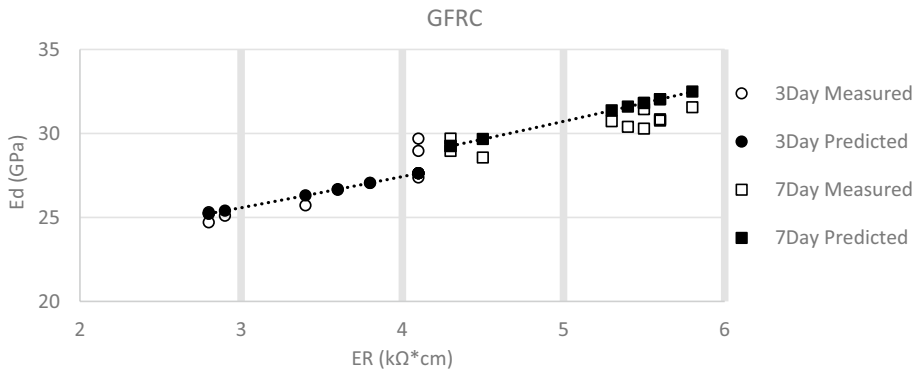

Fig. 9 Correlation between dynamic modulus and electrical resistivity for GFRC.

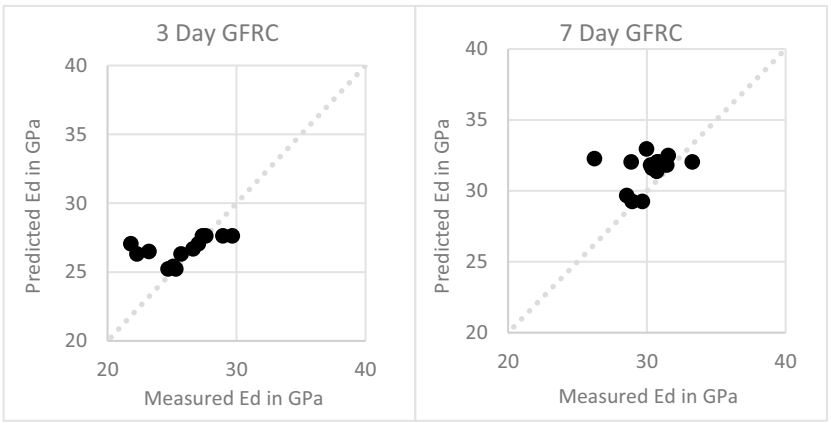

Fig. 10 Correlation between observed Ed and projected Ed for GFRC at early ages.

and the predicted data points were obtained using the adjustment coefficients for GFRC.

The 3-day measured Ed and ER of GFRC range from 24.7 to 27.4 GPa and 2.8–4.1 kΩ * cm, respectively. The 7-day measured Ed and ER of GFRC range from 28.6 to 31.5 GPa and 4.3–5.8 kΩ * cm, respectively.

Fig. 10 compares GFRC's measured Ed to its predicted Ed. Since the COV's at ages 3 and 7 were low, the proposed equation is correct in its early stages.

5 Conclusion

The relationship between dynamic modulus (Ed) and electrical resistivity (ER) of early-age FRC is investigated in this paper by utilizing the NDT methods. A total of 21 mixes were considered at 0.5, 0.75, and 1.00 percent fiber volume fraction (V_f) with w/c ratios of 40%, 45%, and 50% to evaluate this correlation. The electrical properties and dynamic modulus of each fiber were analyzed independently at the ages of 1, 3, 7, and 28 days based on V_f and w/c. It was observed that the electrical resistivity of FRC reduces as the w/c ratio increases at early curing ages for the specific fiber types, w/c ratios, and fiber volume fractions examined in this study. The electrical resistivity of NFRC increased with increasing fiber volume percentage, whereas PFRC, GFRC, and SFRC showed the opposite trend. This is due to an increase in porosity and a decrease in aggregate content, both of which have a significant impact on electrical resistivity. The relationship between the elastic modulus and the electrical resistivity of the studied FRCs has been investigated, and an equation to estimate their correlation at early ages for specific V_f and w/c is proposed. Since elastic modulus and electrical resistivity are both dependent on the porosity of concrete, pore solution conductivity can influence the equation. However, the early age dynamic modulus of elasticity of the four types of FRC can be estimated using the proposed equations, which rely on electrical resistivity and NDT methods. The coefficient of variation (COV) was used to assess the accuracy of the proposed equations for each type of FRC at ages 3 and 7 days. The COVs obtained for predicting the dynamic modulus of the studied FRC using the equations ranged from 6 to 9 percent, demonstrating its reliability.

Acknowledgements
The authors acknowledge the contributions of technical staff at Georgia Southern University, for providing great assistance and helpful comments in executing the experimental program.

Author contributions
All authors contributed to the paper, writing, data analysis and experimental works. All authors read and approved the final manuscript.

Authors' information
Daniel Castillo—Graduate Student, Department of Civil Engineering and Construction, Georgia Southern University, Statesboro, GA, United States. Saman Hedjazi—Assistant Professor, Department of Civil Engineering and Construction, Georgia Southern University, Statesboro, GA, United States. Ehsanul Kabir—Graduate Student, Department of Civil Engineering and Construction, Georgia Southern University, Statesboro, GA, United States.

Funding
There has been no funding for this research.

Availability of data and materials
All the experimental results, material and analysis data are available.

Declarations

Ethics approval and consent to participate
Not applicable.

Consent for publication
Not applicable.

Competing interests
The authors declare that they have no competing interests.

Received: 24 November 2021 Accepted: 19 June 2022
Published online: 10 October 2022

References

American Association of State Highway and Transportation Officials. (2014). *Standard method of test for surface resistivity indication of concrete's ability to resist chloride ion penetration (AASHTO T358)*. AASHTO.
American Concrete Institute. (2014). *Building code requirements for structural concrete (ACI 318)*. American Concrete Institute.
American Society for Testing Materials. (2002). *Standard practice for making and curing concrete test specimens in the laboratory (ASTM C192)*. ASTM International. https://doi.org/10.1520/C0192_C0192M-14
American Society for Testing Materials. (2014). *Standard test method for compressive strength of cylindrical concrete specimens (ASTM C39)*. ASTM Headquarters. https://doi.org/10.1520/C0039_C0039M-14
American Society for Testing Materials. (2015a). *Standard specification for fiber-reinforced concrete (ASTM C1116)*. ASTM Headquarters. https://doi.org/10.1520/C1116_C1116M-10AR15
American Society for Testing Materials. (2015b). *Standard test method for relative density (specific gravity) and absorption of fine aggregate (ASTM C128)*. ASTM International. https://doi.org/10.1520/C0128-01
American Society for Testing Materials. (2015c). *Standard test method for relative density (specific gravity) and absorption of coarse aggregate (ASTM C127)*. ASTM International. https://doi.org/10.1520/C0127-01
American Society for Testing Materials. (2019). *Standard test method for fundamental transverse, longitudinal, and torsional resonant frequencies of concrete specimens (ASTM C215)*. ASTM International.
Appah, D., & Reichetseder, P. (2001). Selection and use of CaO-expanding cements. *Energy Exploration & Exploitation, 19*(6), 581–591. https://doi.org/10.1260/0144598011492697
Aslani, F., & Natoori, M. (2013). Stress-strain relationships for steel fiber reinforced self-compacting concrete. *Structural Engineering and Mechanics, 46*, 295–322. https://doi.org/10.12989/sem.2013.46.2.295
Aslani, F., & Samali, B. (2014). High strength polypropylene fibre reinforcement concrete at high temperature. *Fire Technology, 50*, 1229–1247. https://doi.org/10.1007/s10694-013-0332-y
Ayub, T., Shafiq, N., & Khan, S. U. (2016). Compressive stress-strain behavior of HSFRC reinforced with basalt fibers. *Journal of Materials in Civil Engineering*. https://doi.org/10.1061/(ASCE)MT.1943-5533.0001441
Banyhussan, Q. S., Yıldırım, G., Anıl, Ö., Erdem, R. T., Ashour, A., & Şahmaran, M. (2019). Impact resistance of deflection-hardening fiber reinforced concretes with different mixture parameters. *Structural Concrete, 20*(3), 1036–1050.
Blinder, A. S. (2008). *The concise encyclopedia of economics*. Keynesian Economics.
Chavez, H. L., Alonso-Guzmán, E., Graff, M., & Arteaga-Arcos, J. C. (2014). Prediction of the static modulus of elasticity using four non destructive testing. *Revista De La Construcción. Journal of Construction, 13*(1), 33.
Chavhan, P. P., & Vyawahare, M. R. (2015). Correlation of static and dynamic modulus of elasticity for different SCC mixes. *International Journal on Recent and Innovation Trends in Computing and Communication, 3*(7), 4914–4919.
Danjuschewskij, V. S., & Ghofrani, R. (1991). Volume changes in cement slurries and set cements. *Erdoel Erdgas Kohle (germany)*. https://doi.org/10.4172/2472-0518.1000112
Dopko, M. (2018). *Fiber reinforced concrete: Tailoring composite properties with discrete fibers*. Iowa State University.
Estolano, V., Fucale, S., Vieira Filho, J. O., Gabriel, D., & Alencar, Y. (2018). Assessment of static and dynamic modulus of elasticity in concrete made with recycled aggregate from concrete precast rejects. *Matéria (rio De Janeiro)*. https://doi.org/10.1590/S1517-707620170001.0310
Gowers, K., & Millard, S. (1999). Measurement of concrete resistivity for assessment of corrosion. *ACI Materials Journal, 96*(5), 536.
Guo, Y. X., Ran, H. Y., Feng, G. R., Du, X. J., Qi, T. Y., & Wang, Z. H. (2020). Effects of curing under step-by-step load on mechanical and deformation properties of cemented gangue backfill column. *Journal of Central South University, 27*(11), 3417–3435.
Haque, M. A., & Rasel-Ul-Alam, M. (2018). Non-linear models for the prediction of specified design strengths of concretes development profile. *HBRC J, 14*, 123–136. https://doi.org/10.1016/j.hbrcj.2016.04.004
Kayondo, M., Combrinck, R., & Boshoff, W. P. (2019). State-of-the-art review on plastic cracking of concrete. *Construction and Building Materials, 225*, 886–899.
Kolluru, S. V., Popovics, J. S., & Shah, S. P. (2000). Determining elastic properties of concrete using vibrational resonance frequencies of standard test cylinders. *Cement, Concrete and Aggregates, 22*, 81–89. https://doi.org/10.1520/CCA10467J
Lee, B. J., Kee, S. H., Oh, T., & Kim, Y. Y. (2015). Effect of cylinder size on the modulus of elasticity and compressive strength of concrete from static and dynamic tests. *Advances in Materials Science and Engineering*. https://doi.org/10.1155/2015/580638
Nycon. (2019). *Nycon-AR-DM (Fiberglass) alkali resistant, dry or wet mix, medium denier, superior finish*. Nycon Headquarters.
Olson Instruments. Retrieved February 26, 2020, from https://olsoninstruments.com/
Park, S. J., Yim, H. J., & Kwak, H. G. (2014). Nonlinear resonance vibration method to estimate the damage level on heat-exposed concrete. *Fire Safety Journal, 69*, 36–42.
Pokorny, M., Jendzelovsky, N., & Konecna, L. (2016). Determination of the dynamic modulus of elasticity and the thickness of concrete structures by non-destructive methods. *Key Engineering Materials, 691*, 344–355.
Resipod User's Manual. (2017). *Resipod family operating instruction concrete durability testing*. Proceq USA Inc.
Safari, S. (2016). *Early-age mechanical properties and electrical resistivity of geopolymer composites. Thesis submitted for the award of Master of Philosophy*. Brunel University.
Safiuddin, M., Kaish, A. B. M., Woon, C. O., & Raman, S. N. (2018). Early-age cracking in concrete: Causes, consequences, remedial measures, and recommendations. *Applied Sciences, 8*(10), 1730.
Shao, H., Zhang, J., Fan, T., & Li, Z. (2015). Electrical method to evaluate elastic modulus of early age concrete. *Construction and Building Materials, 101*, 661–666.
Shkolnik, I. E. (2005). Effect of nonlinear response of concrete on its elastic modulus and strength. *Cement and Concrete Composites, 27*(7–8), 747–757.
Skazlić, M., & Bjegović, D. (2009). Toughness testing of ultra high performance fibre reinforced concrete. *Materials and Structures, 42*(8), 1025–1038.
Suksawang, N., Wtaife, S., & Alsabbagh, A. (2018). Evaluation of elastic modulus of fiber-reinforced concrete. *Materials Journal, 115*(2), 239–249.
Tapkın, S. (2008). The effect of polypropylene fibers on asphalt performance. *Building and Environment, 43*(6), 1065–1071.
Teng, S., Afroughsabet, V., & Ostertag, C. P. (2018). Flexural behavior and durability properties of high performance hybrid-fiber-reinforced concrete. *Construction and Building Materials, 182*, 504–515.
Trifone, L. (2017). *A study of the correlation between static and dynamic modulus of elasticity on different concrete mixes*. Statler College of Engineering and Mineral Resources.
Wang, L., He, T., Zhou, Y., Tang, S., Tan, J., Liu, Z., & Su, J. (2021). The influence of fiber type and length on the cracking resistance, durability and pore structure of face slab concrete. *Construction and Building Materials, 282*, 122706.
Wtaife, S., Alsabbagh, A., Essa, T., Alshammari, E., Shaban, A., & Suksawang, N. (2018). Analysis of flexural capacity of fiber reinforced concrete pavements. *International Journal of Technology and Engineering Studies, 4*, 203–210.
Yadav, S., Kusam, A., & Tayebali, A. A. (2021). Evaluating moisture damage using impact resonance test. *Journal of Testing and Evaluation*. https://doi.org/10.1520/JTE20200372
Yuan, J. (2015). Shear strength of reinforced concrete beams. *ACI Structural Journal, 112*(3), 408.

Zeng, X., Liu, H., Zhu, H., Ling, C., Liang, K., Umar, H. A., & Ma, C. (2020). Study on damage of concrete under uniaxial compression based on electrical resistivity method. *Construction and Building Materials, 254*, 119270.

Publisher's Note